Transactions of Tianjin University (2021) 27:295–312
https://doi.org/10.1007/s12209-021-00293-9

REVIEW

Research Progress on Photocatalytic/Photoelectrocatalytic Oxidation of Nitrogen Oxides

Shuangjun Li[1] · Linglong Chen[1] · Zhong Ma[1,2] · Guisheng Li[1,2] · Dieqing Zhang[1]

Received: 31 March 2021 / Revised: 17 April 2021 / Accepted: 2 May 2021 / Published online: 31 May 2021

Abstract

The emission of nitrogen oxides (NO_x) increases year by year, causing serious problems to our livelihoods. The photocatalytic oxidation of NO_x has attracted more attention recently because of its efficient removal of NO_x, especially for low concentrations of NO_x. In this review, the mechanism of the photocatalytic oxidation of NO_x is described. Then, the recent progress on the development of photocatalysts is reviewed according to the categories of inorganic semiconductors, bismuth-based compounds, nitrogen carbide polymer, and metal organic frameworks (MOFs). In addition, the photoelectrocatalytic oxidation of NO_x, a method involving the application of an external voltage on the photocatalytic system to further increase the removal efficiency of NO_x, and its progress are summarized. Finally, we outline the remaining challenges and provide our perspectives on the future directions for the photocatalytic oxidation of NO_x.

Keywords NO_x · Photocatalytic · Photoelectrocatalytic · Mechanism · Photocatalyst

Introduction

The livelihood of human beings, in terms of food, clothing, shelter, and transportation, has greatly improved since the beginning of the industrial revolution. However, the large consumption of fossil fuels, such as coal and petroleum, has led to the excessive emission of nitrogen oxides (NO_x) [1]. The NO_x emitted into the atmosphere not only causes acid rain [2, 3], photochemical smog [4, 5], PM2.5 [6, 7], and other environmental problems but also changes the climate and destroys the ozone layer [8]. In addition, NO_x severely damages the human heart and lungs and further reduces the efficacy of the human immune system [9], making the human body susceptible to respiratory diseases, such as cough, eye inflammation, chest tightness, nausea, sore throat, and bronchitis [10, 11]. Therefore, eliminating NO_x present in the atmosphere is important. Currently, the solutions to remove NO_x mainly are the typical adsorption method [12], nonselective catalytic reduction (NSCR) [13], and selective catalytic reduction (SCR) [14–16]. Most of these methods involve technologies for eliminating NO_x after its generation owing to many obstacles. The adsorption method is suitable only for the removal of a high concentration of NO_x in the combustion exhaust gas, has a high purification efficiency, and does not produce additional liquid wastes; however, it has a high operating cost [17]. Furthermore, NSCR or SCR technologies, in general, are limited to the treatment of high concentrations of NO_x [12, 18], and their efficiency and economic benefits reduce for lower NO_x concentration. Therefore, the low concentration of NO_x, especially in relatively closed places (such as urban streets, tunnels, underground parking lots, and various public indoors), cannot be effectively removed by these traditional methods [19]. The photocatalytic oxidation of NO_x is a green, low-cost method to eliminate NO_x (especially for low-concentration NO_x in the air at room temperature) that has attracted much attention recently [20, 21]. Generally, the photocatalysts in this system absorb light energy and generate separated electrons and holes that further drive the oxidation of NO_x and play the most important role in the

Shuangjun Li and Linglong Chen contributed equally to this work.

✉ Dieqing Zhang
dqzhang@shnu.edu.cn

[1] Key Laboratory of Resource Chemistry of Ministry of Education, Shanghai Key Laboratory of Rare Earth Functional Materials, Joint International Research Laboratory of Resource Chemistry, Ministry of Education , Shanghai Normal University, Shanghai 200234, China

[2] School of Environmental and Geographical Sciences, Wetland Ecosystem Observation and Research Field Station, Shanghai Normal University, Shanghai 200234, China

removal of NO_x. Extensive efforts focused on developing highly active photocatalysts have resulted in a great amount of progress on photocatalysts for oxidation of NO_x in recent years. In this review, the mechanism of the photocatalytic oxidation of NO_x and the design principle of photocatalysts are described. The recent progress on the development of photocatalysts is then reviewed according to the categories of TiO_2-based inorganic semiconductors, bismuth (Bi)-based inorganic semiconductors, graphite-phase carbon nitride and its complexes, and metal organic frameworks (MOFs). In addition, the progress on the development of photoelectrocatalytic oxidation of NO_x is also summarized. We outline the remaining challenges and provide perspectives on future directions for developing photocatalytic oxidation of NO_x.

Mechanism of Photocatalytic Oxidation of NO_x

Under light irradiation, a photocatalyst absorbs a photon (packet of light energy), and its valence band electron is promoted to the conduction band with the hole remaining in the valence band, creating an electron–hole pair. The holes on the valence band (h^+) can oxidize the adsorbed water into OH, and the electrons on the conduction (e^-) band possess the ability to reduce the adsorbed oxygen into superoxide radicals ($\cdot O_2^-$) [22]; these active oxygen species participate in the oxidation of NO_x to produce NO_3^-, NO_2^-, and a small amount of NO_2. The mechanism of photocatalytic oxidation of NO_x is depicted in Fig. 1, and its specific reaction pathway is described as follows as Eqs. (1–6):

$$\text{Photocatalyst} + h\nu \rightarrow e^- + h^+ \quad (1)$$

$$e^- + O_2 \rightarrow \cdot O_2^- \quad (2)$$

$$h^+ + OH^- \rightarrow \cdot OH \quad (3)$$

$$NO + \cdot O_2 \rightarrow NO_3^- \quad (4)$$

$$\cdot OH + NO \rightarrow HNO_2 \quad (5)$$

$$HNO_2 + \cdot HO \rightarrow HNO_3 \quad (6)$$

Based on the above mechanism, the effectiveness of photocatalytic oxidation of NO_x is mainly dominated by photocatalyst. Firstly, electron–hole pair generation in photocatalysts is the trigger for the oxidation of NO_x, and this generation mainly depends on whether the band gap of the photocatalyst matches the wavelength of the absorbed light. For example, TiO_2 with a band gap of only 3.2 eV can be excited to produce electron–hole pairs under the UV-light irradiation with a wavelength less than 380 nm. However, UV light only accounts for 3%–5% of sunlight, whereas the proportion of visible light in sunlight can reach up to 43%. To use visible light, new photocatalysts with a small band

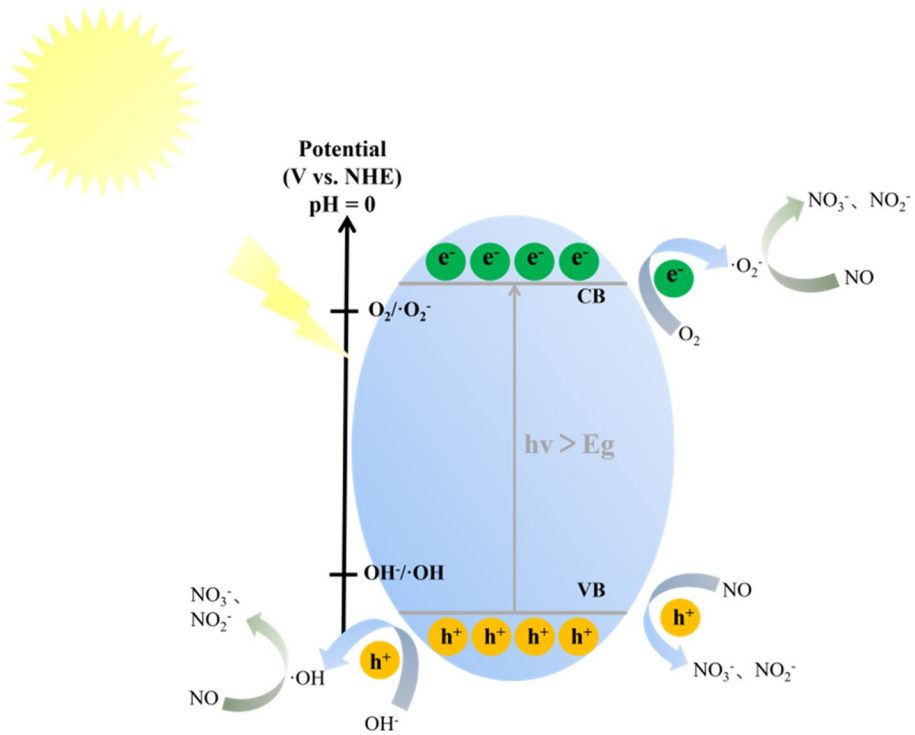

Fig. 1 Mechanism of photocatalytic oxidation of NO_x (Reproduced with permission from Ref. [22]. Copyright 2016 Elsevier)

gap should be developed. Further, the lifetime of photogenerated electrons and holes also affects the efficiency of NO conversion. For example, the photogenerated holes only have a lifetime of 10^{-9} s; this short lifetime severely decreased the occurrence of reaction between these active species and NO_x. In addition, the charge transfer rate of a photocatalyst is also critical. Thus, extensive research has been focused on developing powerful photocatalysts by decreasing their band gaps and slowing down their recombination rates of electrons and holes.

Recent Progress on Photocatalysts for Treating NO Gas

Since 1994, when Ibusuki and Takeuchi [23] firstly applied photocatalytic technology to the removal of NO_x, extensive attention has been devoted to this field, with several photocatalysts developed and evaluated toward oxidizing NO_x. Currently, the reported photocatalysts could be classified mainly into four categories: (1) TiO_2-based inorganic semiconductors [24–26], (2) Bi-based inorganic semiconductors [27, 28], (3) graphite-phase carbon nitride and its complexes [29], and (4) MOFs [30] (Fig. 2); recent progress in the development of these photocatalysts is summarized in the following section (Table 1).

TiO_2-Based Semiconductors

Titanium oxide (TiO_2), a white, odorless, nontoxic powder, is a representative candidate of an inorganic semiconductor photocatalyst; TiO_2 possesses three types of crystal structures: anatase, rutile, and brookite [20]. TiO_2 is mainly divided into anatase and rutile phases [24]. Anatase TiO_2 has a wide band gap (3.2 eV), which can be excited only by UV light, resulting in a very low utilization of sunlight. Furthermore, the high recombination probability of photogenerated carriers for TiO_2 is not conducive to its wide application in the field of photocatalysis (PC). A study has found that the mixed crystals of anatase and rutile presented excellent photocatalytic activity because of the internal electric field formed between the two types that facilitated the separation of electrons and holes [25]. Gong and Selloni [31] revealed that the (001) facet of anatase has much higher activity than the (101) facet by theoretical calculations because the defect caused by the unsaturated coordination of Ti atoms on the (001) facet can increase the energy of the crystal surface. Subsequently, some experimental results have verified this

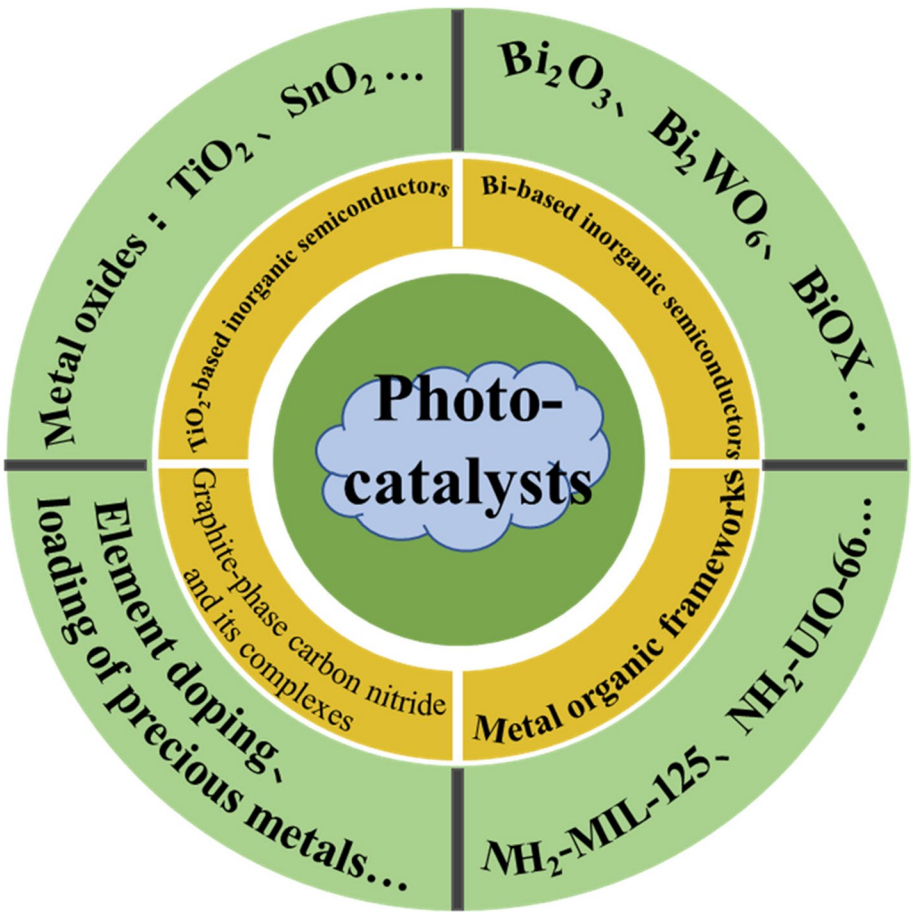

Fig. 2 Classification of photocatalysts toward the oxidation of NO_x

Table 1 Reported photocatalysts for the oxidation of NO_x

No	Photocatalysts	Light types	η(NO) (%)	Active species	Ref
1	Ag NCs/TiO_2	Visible light	63	$\cdot O_2^-$, h^+	[39]
2	Blue Fe-TiO_2	Simulated sunlight	69	$\cdot O_2^-$, h^+, ·OH	[40]
3	SnO_2/TNTs	Visible light	59	$\cdot O_2^-$, ·OH	[26]
4	CNTs-TiO_2	UV light	86	$\cdot O_2^-$, h^+	[41]
5	Ni-Bi_2O_3-5	Simulated sunlight	52	·OH, $\cdot O_2^-$	[28]
6	12% BP/MBWO	Visible light	67	$\cdot O_2^-$, h^+, ·OH	[46]
7	BiOCl-OVs	Simulated sunlight	38	$\cdot O_2^-$, ·OH	[52]
8	Bi-HBPO-102	Visible light	51	$\cdot O_2^-$, h^+, ·OH	[59]
9	Bi/$Bi_2O_{2-x}CO_3$	Visible light	51	h^+, ·OH, H_2O_2	[61]
10	Sr-doped g-C_3N_4	Visible light (300 W Xe lamp)	55	$\cdot O_2^-$, ·OH	[69]
11	$PdCl_2$/mgp-CN	30 W LED ($\lambda \geq 420$ nm)	66	$\cdot O_2^-$, $\cdot h^+$	[70]
12	g-C_3N_4/MS	A 150 W metal halide lamp ($\lambda \geq 420$ nm)	79	$\cdot O_2^-$, h^+, ·OH	[71]
13	N_{2c}-deficient g-C_3N_4	300 W Xe lamp ($\lambda \geq 420$ nm)	33	$\cdot O_2^-$	[72]
14	g-C_3N_4/$Bi_4O_5I_2$	Tungsten halogen lamp ($\lambda \geq 420$ nm)	51	$\cdot O_2^-$, $\cdot h^+$	[76]
15	Ag@NH_2-MOP(Ti)	Tungsten halogen lamps ($\lambda \geq 420$ nm)	53	$\cdot O_2^-$, ·OH	[30]
16	GO/NH_2-MIL-125	Tungsten halogen lamps ($\lambda \geq 420$ nm)	65	·OH,$\cdot O_2^-$	[87]
17	Cu-NU7	150 W tungsten lamps ($\lambda \geq 420$ nm)	88	$\cdot O_2^-$, h^+	[88]
18	TiO_2-CNT/SSMs	UV light	60	h^+, ·OH	[92]
19	TiO_2 nanorod array/FTO	UV light	81	h^+, ·OH	[100]

viewpoint [32–34]. However, the surface of the (001) facet requires special means to be stable because it has higher surface energy [35]. For instance, Yang et al. [34] found that the fluorine atom can significantly reduce the energy of the surface (001), making it even more stable than the surface (101). As a result, they made a breakthrough in using fluorine atom as the capping agent to synthesize micron-size TiO_2 single crystals with (001) facet as the main crystal [36–38]. Han et al. [37] synthesized a rectangular TiO_2 nanosheet with highly reactive (001) top and bottom surfaces using a simple hydrothermal approach with the aid of hydrofluoric acid solution. Owing to the exposure of a high percentage of (001) facets, this TiO_2 nanosheet exhibited excellent photocatalytic efficiency that far exceeds that of the commercial P25. In addition, Chen et al. [38] used a solvothermal method to construct a (001) facet exposed TiO_2 and porous graphene composite; this highly active (001) surface and excellent interface interaction in these unique three-dimensional (3D) structures provided a significant high-efficiency photocatalytic activity because of the effective molecular oxygen activation along with rapid in-plane and vertical light-induced charge transfer. Moreover, precious metal deposition, metal ion doping, and constructing semiconductor mixtures have also been used to modify TiO_2 to improve its photocatalytic activity. Duan et al. [39] prepared Ag NCs/TiO_2 composites by depositing Ag nanoclusters (NCs) onto TiO_2 nanoparticles. The electrons generated from lowest unoccupied molecular orbital (LUMO) of Ag NCs migrated to the conduction band of TiO_2 and induced the production of superoxide radicals that can efficiently oxidize NO (Fig. 3a) under visible light irradiation. The photocatalytic activity toward NO oxidation is three and two times that of pure TiO_2 and Ag NC_S, respectively (Fig. 3b).

Furthermore, the work of Duan et al. effectively inhibited the formation of toxic byproduct, NO_2, and exhibited excellent stability [39]. Using the metal-ion doping method, Martinez-Oviedo et al. [40] synthesized Fe- or Cu-doped reduced blue TiO_2 using Li in the ethylene-diamine (EDA) process. The photocatalyst with the incorporation of Fe showed the best photocatalytic performance among these doped photocatalysts because of the reduced band gap (Fig. 3c, d), increased visible-light absorption capability, the existence of oxygen vacancies/Ti^{3+} species, and efficient separation efficiency of photogenerated carriers. The structured SnO_2/TiO_2 photocatalysts were fabricated by loading SnO_2 nanoparticles onto TiO_2 nanotubes (TNT) with the formation of SnO_2/TNTs heterojunctions through a one-step hydrothermal method [26]. As shown in Fig. 3e, the electrons generated in each TNT migrated to the conduction band of SnO_2, whereas the holes in SnO_2 valence band migrated to the valence band of TNTs. In that case, the recombination rate of photogenerated electron–hole pairs was effectively reduced, allowing the photocatalytic oxidation efficiency of NO to reach up to 60%. Moreover, the production of NO_2 was inhibited in this photocatalysis. Apart from the above methods, Zhang et al. [41] developed a general microwave antenna strategy to synthesize the discontinuous distribution of nano-semiconductors through carbon nanotubes (CNTs)

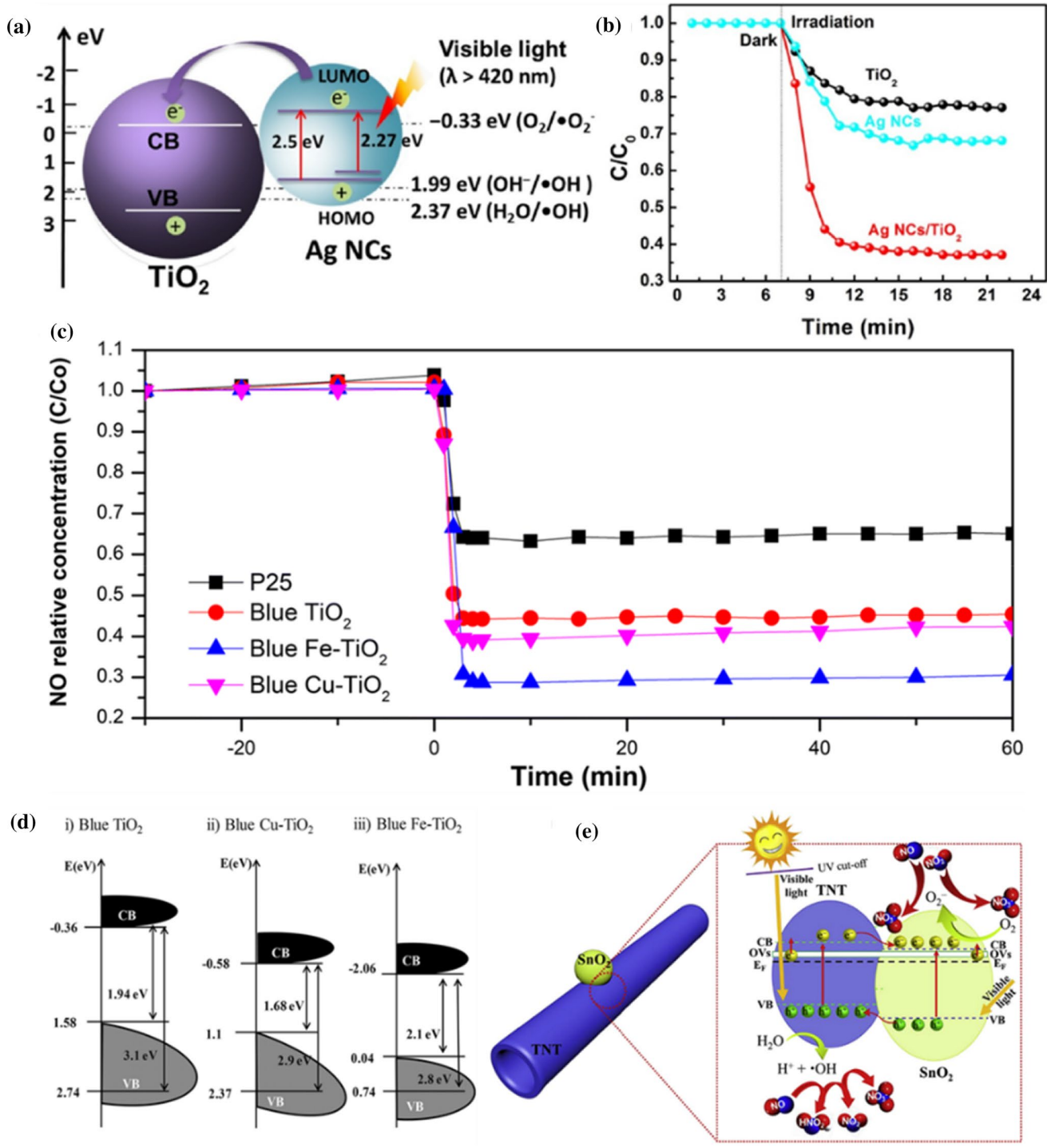

Fig. 3 **a** Electron transfer pathway of Ag NCs modified TiO_2; **b** NO oxidation reaction profiles of TiO_2, Ag NCs, and Ag NCs/TiO_2 (Reproduced with permission from Ref. [39]. Copyright 2018 Elsevier); **c** the calculated band edges of blue TiO_2, blue Cu-TiO_2, and blue Fe-TiO_2; **d** the enhancement of NO_x photo-oxidation by Fe- and Cu-doped blue TiO_2 (Reproduced with permission from Ref. [40]. Copyright 2020 Springer-Verlag GmbH Germany); **e** the structure and photocatalytic mechanism of SnO_2/TNT (Reproduced with permission from Ref. [26]. Copyright 2018 Elsevier)

via imitating chloroplasts (Fig. 4a, b). The cross-linked CNTs in this hybrid catalyst provided an efficient dual electron transfer pathway, i.e., the intimate "line-contact" among CNTs, TiO_2 microspheres, and the 3D CNTs conductive networks. For such a catalyst, a close "linear-contact" between CNTs and TiO_2 was built through the covalent bonds of

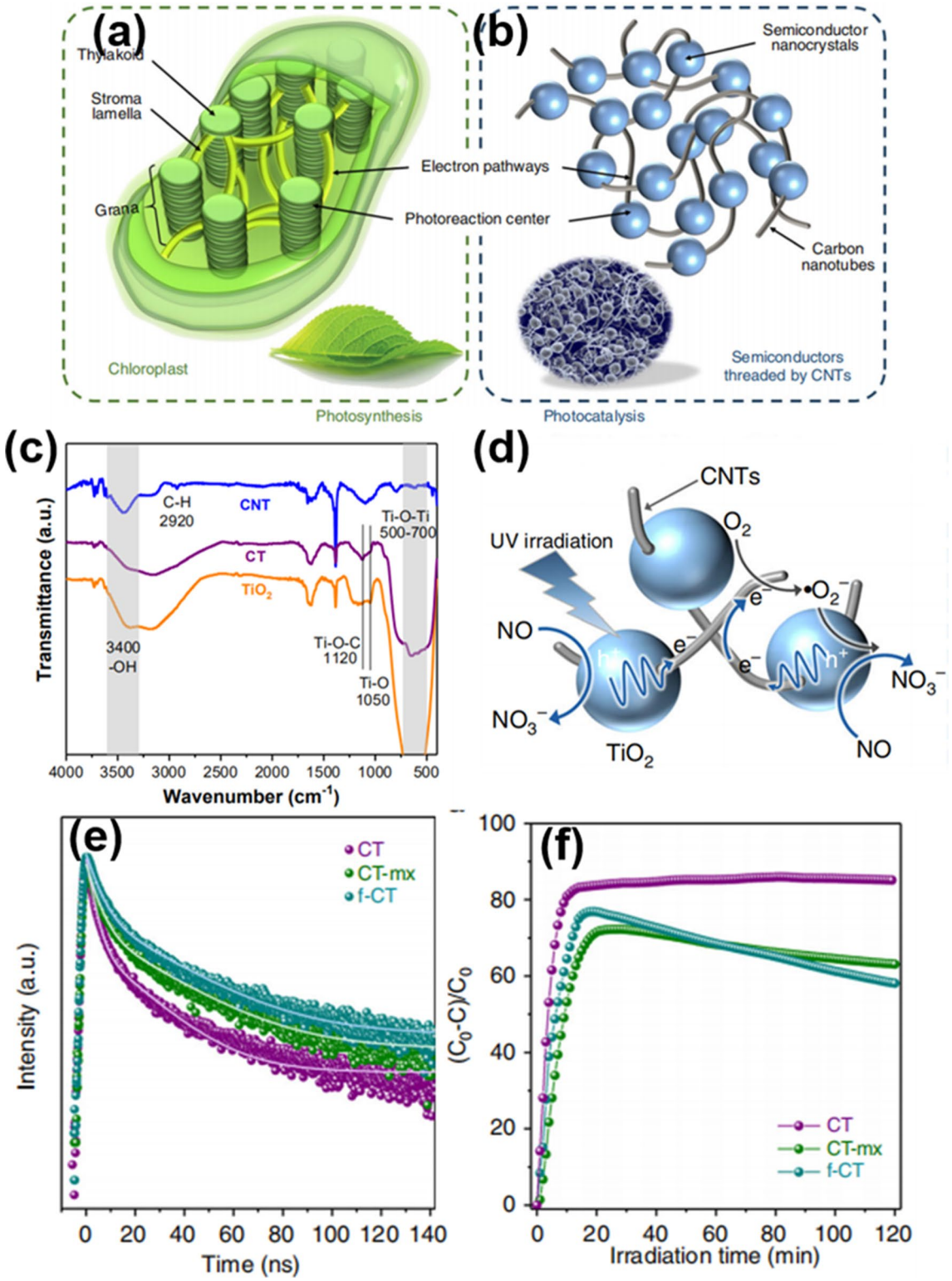

Fig. 4 **a** Top view of the chloroplast structure; **b** discontinuous structure of the distributed semiconductors with carbon-nanotube threads; **c** FT-IR spectra of the sample CT, pure TiO_2 and CNT; **d** the photosynthesis mechanism of the chloroplast (left) and the photocatalytic NO removal mechanism of the chloroplast structured CNTs–TiO_2; **e** time-resolved transient photoluminescence decay profiles of samples CT (CNTs/TiO_2), f-CT (the completely encapsulated core–shell structure of CNTs–TiO_2), and CT-mx (the mechanical mixing of CNTs and TiO_2 microspheres); **f** UV-light-driven photocatalytic NO oxidation performances (Copyright 2019 The Author(s))

Ti–O–C = O or Ti–O–C (located at ~ 1120 cm^{-1}) via the carboxyl/hydroxyl groups on the surface of CNTs and TiO_2 during the synthesis process (Fig. 4c). As shown in Fig. 4d, this catalyst was excited by UV light to produce photon-generated carriers (e^- and h^+) in the TiO_2 microspheres. The generated e^- and h^+ can be further effectively separated through this linear-contact by transferring the electrons from TiO_2 to a CNT. In that case, several accumulated electrons on the CNTs could react with O_2 to form a high concentration of oxidant radicals ($\cdot O_2^-$) that can react with NO. As shown in Fig. 4e, f, the CT sample was found to prolong the carrier life, with its NO conversion rate under UV irradiation being as high as 86% with good reaction stability.

Bi-Based Inorganic Semiconductors

Bi-based photocatalysts mainly include unary metal Bi-based compounds, binary metal Bi-based compounds, bismuth oxyhalide compounds, bismuth phosphate, bismuth vanadate compounds, and bismuth oxycarbonate [27, 42, 43]. The monometallic Bi-based photocatalysts (Bi_2O_3 and Bi_2S_3) are the simplest Bi-based compounds, with the band gap ranging from 2.00 to 3.96 eV, which can be excited by visible light. Lei et al. [43] introduced oxygen vacancies into the β-Bi_2O_3 catalyst; after optimization, under visible light irradiation, the photocatalytic NO removal rate of defective β–Bi_2O_3 increased from 25.2% to 52.0%. Dong et al. [28] prepared two types of Ni-doped Bi_2O_3 microsphere (Ni–Bi_2O_3–5 and Ni–Bi_2O_3–2) photocatalysts through a one-pot solvothermal method (Fig. 5a–d); the two catalysts exhibited much higher photocatalytic activities, 52% and 35% for Ni–Bi_2O_3–5 and Ni–Bi_2O_3–2, respectively, compared to 31% for the pure Bi_2O_3 sample because the doped Ni changed the geometric and electronic structure. In addition, Ni–Bi_2O_3–5 showed no obvious activity drop after five cycles (Fig. 5e, f).

Besides Bi_2O_3, Bi_2WO_6-based semiconductors have also been proven as effective photocatalysts for oxidizing NO_x owing to their special crystal structures [44, 45]. However, the photocatalytic activity of traditional 3D Bi_2WO_6 is not satisfactory because of the rapid recombination of electron–hole pairs, the narrow visible light response range, and the low specific surface area resulting in the low exposure of active sites. Hu et al. [46] prepared a Z-type heterojunction of 2D/2D black phosphorus/single layer Bi_2WO_6 as a 2D nanosheet catalyst that exhibited high specific surface area (Fig. 6a, b), many active sites, and a unique electronic structure; this catalyst achieved 67% visible-light catalytic activity for removing NO and long-term stability (Fig. 6c, d).

Bismuth oxyhalide, as an important Bi-based semiconductor, possesses excellent optical properties owing to its layered structure consisting of a double layer of interlaced halogen atoms $[Bi_2O_2]^{2+}$. Recently, p-block bismuth oxyhalides (BiOX, X = Cl, Br, I) have attracted widespread attention because of its unique polar two-dimensional (2D) layered crystal structure [47–51]. He et al. [42] designed a novel Bi quantum dot (QDS)-injected C-doped BiOCl photocatalyst (C/BOC/B) that had a NO_x removal efficiency that reached the maximum value of 53.0% within 8 min, with no significant attenuation observed after continuous irradiation, indicating the modification of Bi QDS can further improve the photocatalytic performance of the C/BOC catalyst. Dong et al. [52] prepared BiOCl nanosheets with oxygen vacancies by reconstructing hydrophobic BiOCl. Because oxygen vacancies possess electron trapping ability and promote the separation of light-excited charges, BiOCl nanosheets showed enhanced visible light absorption. For example, under simulated sunlight, the defective BiOCl exhibited a NO removal rate of 38%, which is much higher than that of BiOCl (27%), attributed to the increased carrier density and charge separation performance. Under visible light (≥ 420 nm), the defective BiOCl exhibited 11% NO removal activity, whereas BiOCl only possessed a negligible NO removal rate. This work also revealed the correlation between atomic defects and photocatalytic performance and provided the inspiration for the design and manufacture of photocatalysts. Bismuth phosphate ($BiPO_4$) contains acid radical ions, with the oxygen located in the acid radical rather than the metal oxygen structure; this configuration can greatly promote the separation of photogenerated electrons and holes [53]. Thus, $BiPO_4$ has been widely used for driving photocatalytic reactions. Generally, $BiPO_4$ has two crystal structures, hexagonal and monorhombic; these crystal structures have different light absorption and charge transferability because of their distinguished surface atoms arrangements [54–57]. Furthermore, the plasmon resonance effect was combined with $BiPO_4$ via loading metallic Bi, which can be used as an electron donor [58, 59]. Dong et al. [59] observed that the deposition of Bi metal on the (102) facet of the defective hexagonal $BiPO_4$ (Fig. 7a) resulted in a 51% NO removal rate, much higher than that of the Bi metal decorated on the (120) facet of the defective monoclinic $BiPO_4$ (36%) (Fig. 7b). In addition, with the synergistic effect of the surface plasmon resonance effect and phosphoric acid defect, a new mechanism for electron transmission from $[Bi_2O_2]^{2+} \rightarrow$ Bi metal $\rightarrow PO_4^{3-}$ was constructed on Bi-$BiPO_4$ catalyst (Fig. 7c). $B(BiO)_2CO_3$ belongs to the Oliviers-related oxide family, with a layered structure of Bi_2O_2 and CO_3^{2-} layers interlaced with each other [22]. The interface between the $[Bi_2O_2]^{2+}$ and CO_3^{2-} layer can promote the separation of light-induced electron–hole pairs, thereby improving its quantum efficiency; however, the production of NO_2 was found to be typically present [60]. To address this problem, Huang et al. [61] synthesized Bi/$Bi_2O_{2-x}CO_3$ nanosheets with abundant oxygen

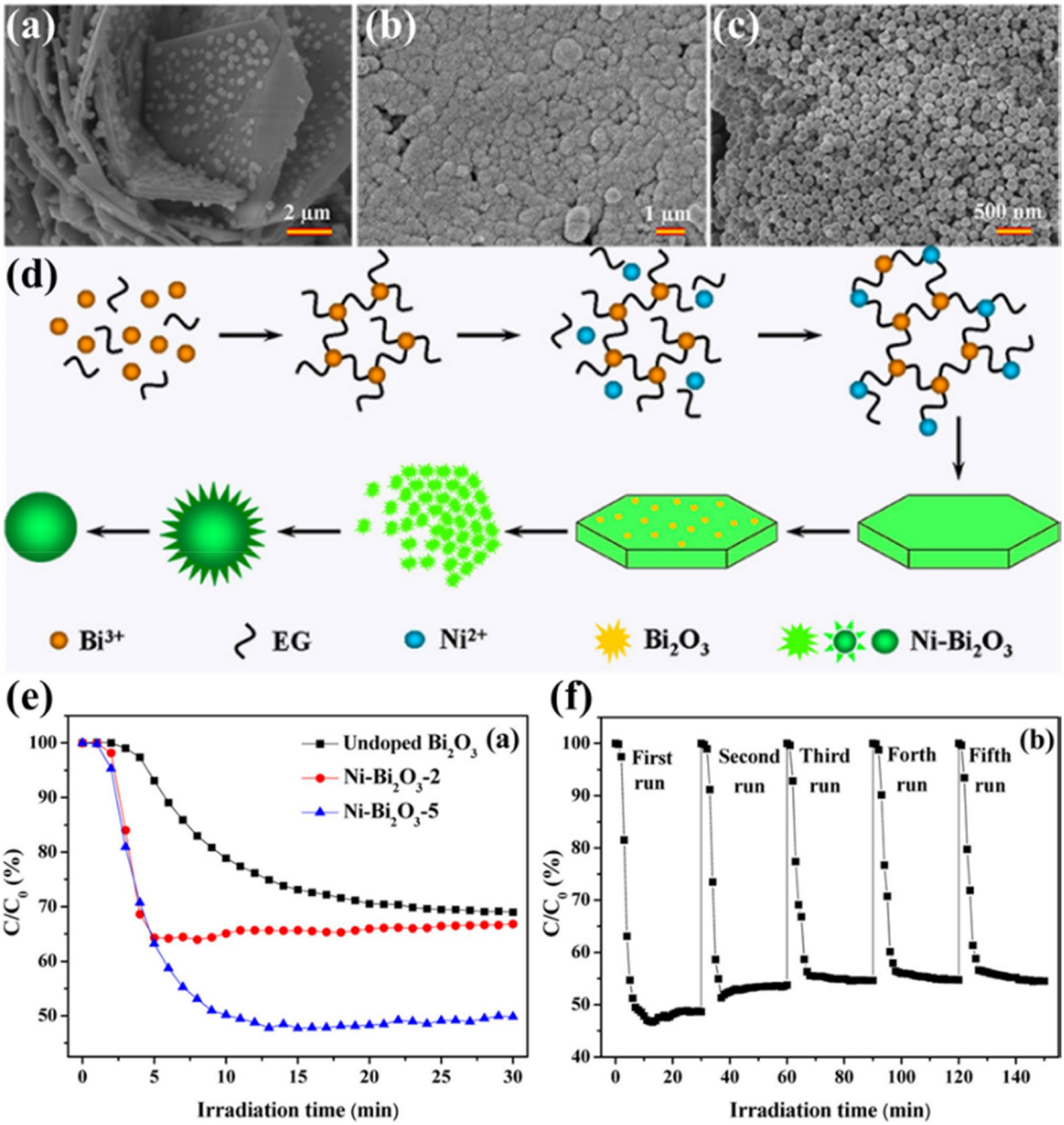

Fig. 5 SEM images of **a** undoped Bi_2O_3; **b** Ni-Bi_2O_3-2, and **c** Ni-Bi_2O_3-5; **d** schematic illustration of the proposed formation mechanism of Ni-Bi_2O_3 microspheres; **e** photocatalytic performances of Bi_2O_3, Ni-Bi_2O_3-2, and Ni-Bi_2O_3-5; **f** multiple photocatalytic reaction over Ni-Bi_2O_3-5 (Reproduced with permission from Ref. [28]. Copyright 2017 American Chemical Society)

vacancies on the surface. The removal rate of NO for these nanosheets under visible light was found to be as high as 51%, and the selectivity for NO_3^- was found to reach up to 98% (Fig. 7d, e). With the Bi plasma resonance, hydrogen peroxide was generated through two electrons path on this catalyst; thus, the generation of NO_2 was inhibited. Furthermore, the oxygen vacancies between the Bi–O layers acted as an electron transfer channel between Bi and $Bi_2O_{2-x}CO_3$, improving the separation rate of photogenerated carriers and thus, the photocatalytic efficiency.

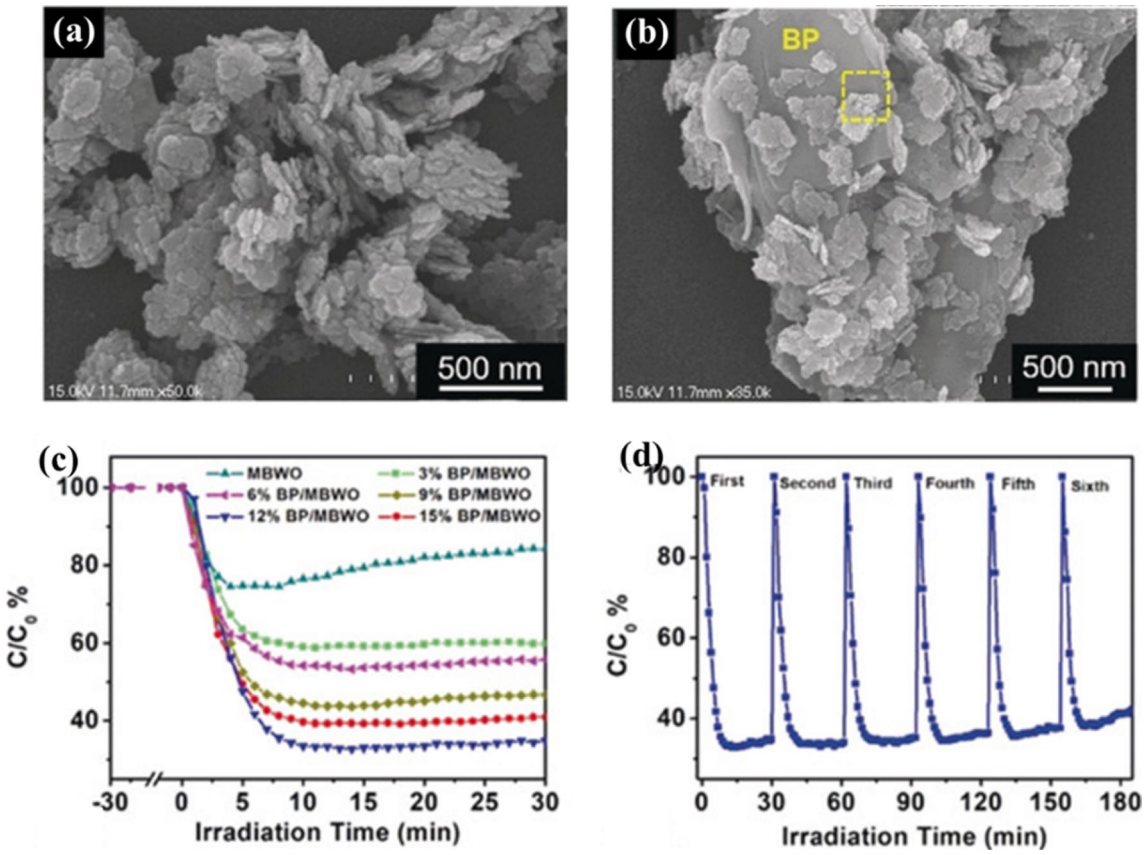

Fig. 6 SEM images of **a** MBWO (monolayer Bi_2WO_6) nanosheets; **b** 12% BP/MBWO (black phosphorus and monolayer Bi_2WO_6) heterojunctions; **c** the relevant photocatalytic NO removal rates; **d** multiple cycles of photocatalytic reactions over 12% BP/MBWO (Reproduced with permission from Ref. [46]. Copyright 1999–2021 John Wiley & Sons, Inc.)

Graphite-Phase Carbon Nitride and Its Complex

Graphite-phase carbon nitride (g-C_3N_4) is a nonmetallic, polymer semiconductor photocatalytic catalyst that has many advantages, including small band gap width of 2.7 eV, visible light photocatalytic activity, low cost, good acid and alkali corrosion resistance, and excellent chemical and thermal stabilities [20, 29, 62–64]. However, the low separation efficiency of photogenerated electron–hole pairs and poor visible-light utilization efficiency of g-C_3N_4 limit its applications in PC [65]. Studies have revealed that the photocatalytic activity of g-C_3N_4 toward removing low-concentration NO_x can achieve very high efficiency through elemental doping [66], loading precious metals [67], or morphology tuning [68]. For example, Zhou et al. [69] modified g-C_3N_4 by Sr embedding, Sr replacing N atoms, and Sr filling holes; all these Sr-doped catalysts reduced the band gap of g-C_3N_4 and thus improved the NO removal efficiency under visible light, and effectively inhibited the production of NO_2. More specifically, the multisite doping of Sr could improve the NO removal rate by 1.5 times while reducing the conversion rate of NO_2 from 63% to 16%. Zhang et al. [70] developed a simple and efficient molecular/solid hybrid photocatalyst composed of noble metal (such as Au^{III}, Pt^{IV}, and Pd^{II}) chlorides, and mesoporous graphite carbon nitride (mpg-CN). Adding $PdCl_2$ improved the photocatalytic ability of mpg-CN and increased the efficiency from 32% to 65% for the photocatalytic removal of 1000 ppb of NO. Li et al. [64] reported a C_3N_4 supported Pd nanoparticles catalyst (PdCN) for photocatalytic oxidation of NO_x; this PdCN was found to have a better purification effect on NO in the air, reaching a maximum of 51.5% in the first 5 min, followed by stabilization at 44.9%. Yang et al. [71] successfully synthesized a g-C_3N_4/melamine sponge (g-C_3N_4/MS) using the ultrasonic coating method with g-C_3N_4 uniform dispersion and immobilization on the melamine skeleton (Fig. 8a–d). The g-C_3N_4/MS composite still possessed the porous structure of MS, and its specific surface area was much larger than that of the photocatalyst in powder form. In that case, g-C_3N_4/MS exposed more active sites, enhanced visible light absorption, and enhanced separation of photogenerated carriers; the NO removal rate reached 79% in the first 5 min under visible-light irradiation, which was

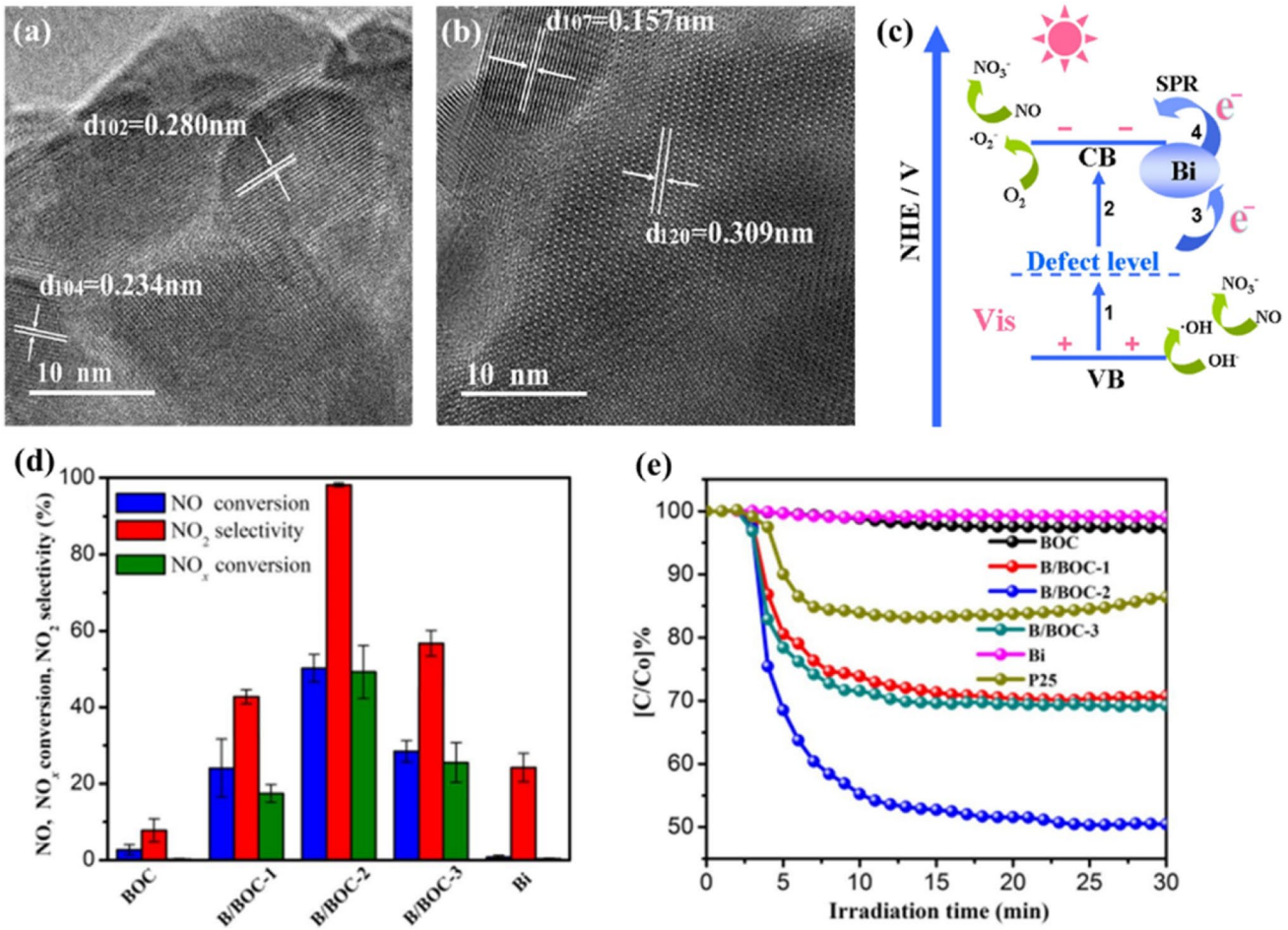

Fig. 7 **a** HRTEM image of Bi-HBPO-102; **b** HRTEM image of Bi-MBPO-120 (Reproduced with permission from Ref. [59]. Copyright 2018 Elsevier); **c** proposed photocatalytic mechanism on Bi-HBPO-102 and Bi-MBPO-120; **d** photocatalytic NO removal efficiencies (C/C_0) of as-prepared samples; **e** NO, NO_x conversion and NO_2 selectivity obtained for catalysts subjected to 30 min irradiation (Reproduced with permission from Ref. [61]. Copyright 2019 Elsevier)

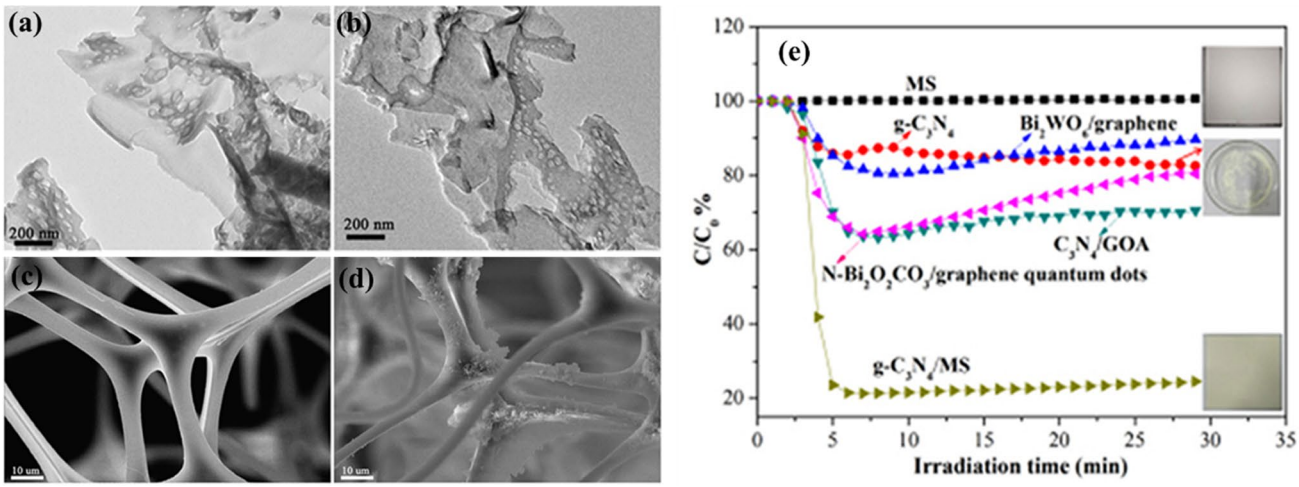

Fig. 8 TEM images of samples: **a** g-C_3N_4; **b** sonicated g-C_3N_4; SEM images of **c** MS and **d** g-C_3N_4/MS; **e** NO removal ratios of various samples (Reproduced with permission from Ref. [71]. Copyright 2018 The Author(s))

approximately 4.5 times that of the powder g-C_3N_4 (18%), whereas the original MS did not work for the removal of NO (Fig. 8e).

In addition, the photocatalytic activity of g-C_3N_4 can be significantly improved by the introduction of defects [72]. Wang et al. [73] prepared g-C_3N_4 microtubes with adjustable N vacancy concentration using the in situ soft chemical method (Fig. 9a, b). They found the surface N-vacancies not only acted as the specific sites for the adsorption, activation of the reactants, and photoinduced electron capture but also enhanced the light absorption capacity of g-C_3N_4, both of which increased the photocatalytic removal efficiency of NO. Under visible-light irradiation, the NO removal rate of CNT-12 was found to reach 33%, which was maintained after five runs (Fig. 9c, d).

Liao et al. [74] also introduced nitrogen defects into the framework of g-C_3N_4 by heating the material in powder form in a hydrogen atmosphere; the NO removal rate on this catalyst was 2.6 times that of the original one because of its much narrower band gap, which can promote the separation of photoexcited charge carriers and generate active oxygen more efficiently under visible-light irradiation. In addition, Ma et al. [75] reported that the combination of metal oxides could improve the specific surface area of g-C_3N_4 and promote the separation of photogenerated electrons and holes, and thus, improve its photocatalytic activity. They prepared g-C_3N_4–TiO_2 composites using commercial P25 and melamine as precursors through a simple calcination route and found the interface interaction between g-C_3N_4 and TiO_2 increased the separation efficiency of photogenerated electrons and holes and generated more active species. Tian et al. [76] also used a hybrid calcination method to build a g-C_3N_4/$Bi_4O_5I_2$ 2D–2D heterojunction nanosheet photocatalyst that showed an enhanced photocatalytic activity of NO removal (with the rate of 51% after 30 min of irradiation) compared with the original g-C_3N_4 and $Bi_4O_5I_2$ under visible light ($\lambda \geq 420$ nm) because of the promoted separation and transfer of photogenerated electron–hole pairs.

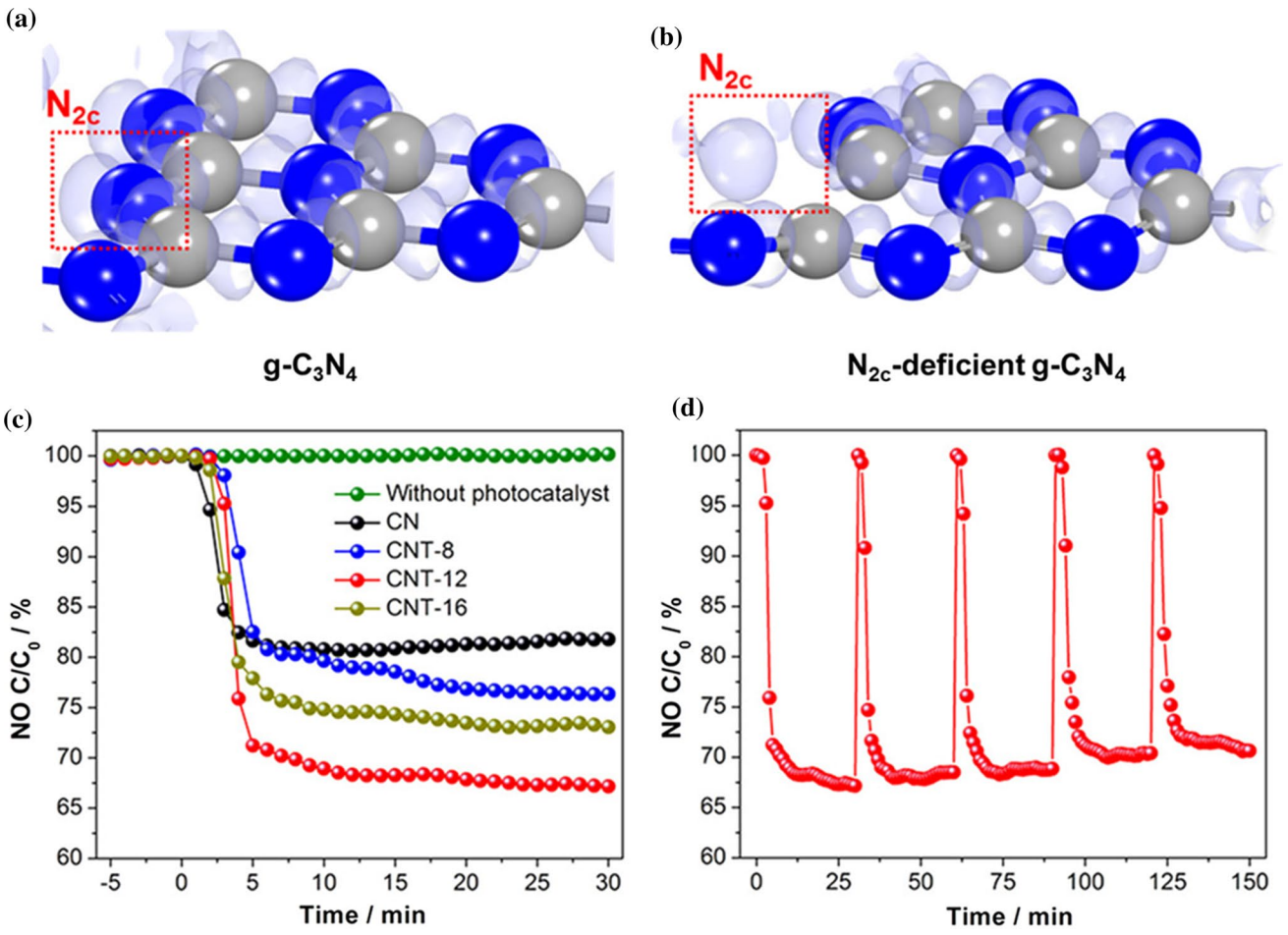

Fig. 9 Calculated electron density difference (EDD) diagrams of g-C_3N_4 **a** and N_{2c}-deficient g-C_3N_4 **b**; visible-light photocatalytic activities of CN, CNT-8, CNT-12, and CNT-16 toward NO removal in air **c**; cycling of CNT-12 during NO removal **d** (Reproduced with permission from Ref. [73]. Copyright 2019 American Chemical Society)

MOFs

Extensive strategies have been devoted to enhancing the activities of traditional photocatalysts toward the oxidation of NO_x, especially for photoexcitation in the visible-light spectral region, including the introduction of heteroatoms, the creation of vacancies (such as O vacancies and N vacancies) [77], metal plasmon resonance [78], and combination of dyes (PI-g-C_3N_4) [79]. However, these catalysts still face many shortcomings, such as the small surface area, limited gas adsorption capacity, low catalytic activity, and easy inactivation. Furthermore, NO_2, a chemical more toxic than NO, can easily accumulate at the surface of these catalysts. The MOFs, formed by connecting inorganic metal oxygen clusters as nodes with organic ligands, usually have super large surface areas, and thus, possess high gas adsorption capacities. For example, Yang et al. [80, 81] found that the Manchester Framework Materials (MFM-520 and MFM-300(Al)) exhibited a high adsorption capacity of 4.2 mmol/g (298 K, 0.01 bar) and 14.1 mmol/g, respectively, for NO_2 uptake under environmental conditions. Moreover, MFM-300(Al) showed a highly selective removal of gas mixtures at low concentrations of NO_2 (1–5000 ppm). Such superiority offered MOFs with promise for use in the photocatalytic oxidation of NO_x [82–86]. In 2015, Zhang et al. [30] synthesized the MOF-like material Ag@NH_2-MOP(Ti) using the microwave-assisted method; that photocatalyst showed excellent photocatalytic activity for oxidizing NO gas, with two times higher activity than that of N-doped TiO_2. In 2018, Zhang et al. [87] further reported the use of the microwave method to produce a new photocatalyst, GO/NH_2–MIL-125, with high crystalline monodisperse NH_2–MIL-125 on the surface of graphene. The strong interaction between MOFs and graphene not only enhances its visible-light absorption but also improves the separation efficiency of photogenerated electrons/holes; thus, the NO_x removal rate on this catalyst can reach 50% under visible-light irradiation ($\lambda \geq 420$ nm). In addition, Zhang et al. [88] found that the Cu species with mixed valence states in NH_2–UIO-66 constructed a new ligand-linker metal Cu charge transfer pathway (LMCT), allowing electrons to be transferred from the organic linker to the Cu center (Fig. 10a). This novel electron transfer pathway prolonged the life of photogenerated electrons under visible light, making the activity of this catalyst as high as 88% and inhibiting the production of NO_2. In addition, these catalysts showed excellent stability (Fig. 10b).

Photoelectrocatalysis Routes for Removing NO_x

Compared with the traditional NO_x treatment process, the PC route has received extensive attention in the field of environmental purification because of its strong oxidation ability, low cost, and environmental friendliness [89–91]. However, the difficult separation and rapid recombination of photogenerated holes and electrons lead to the low NO conversion rate, poor stability, and the production of more toxic NO_2 sometimes, all of which restrict its applications for NO_x removal [92]. In 1972, Fujishima and Honda [93] coated N-type semiconductor TiO_2 onto the electrode and achieved good water decomposition ability under the synergistic action of an external voltage. Subsequently, photoelectrocatalysis attracted widespread attention [94] and has proved effective for the removal of organic pollutants [93],

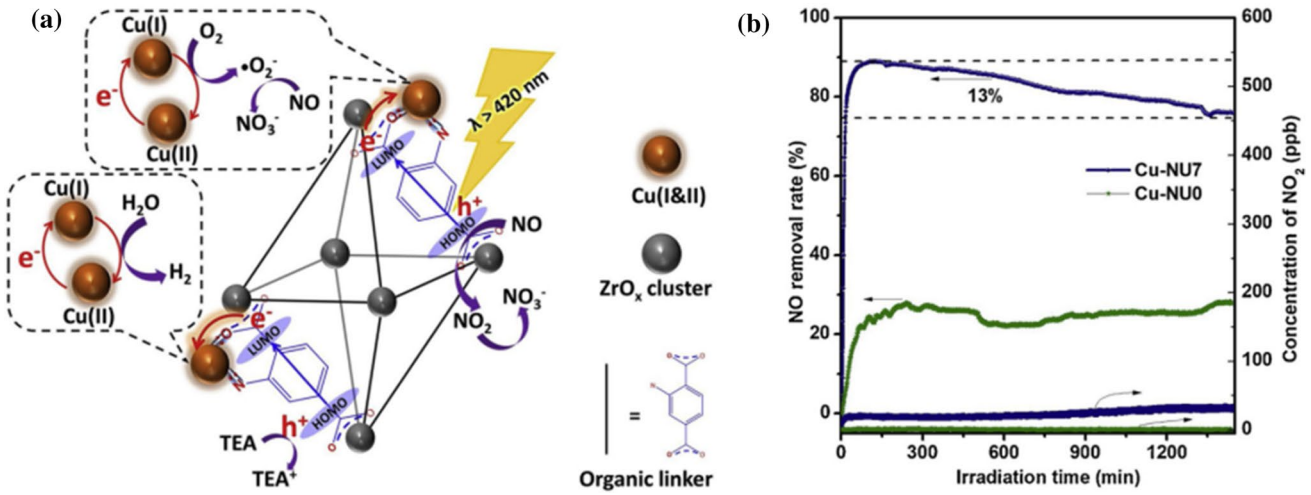

Fig. 10 **a** The proposed mechanism for photocatalytic NO oxidation in the gas phase of CuNU7 (Cu–NH_2–UiO-66(Zr)); **b** the durability test of CuNU7 and Cu-NU0 (NH_2–UIO-66) for the photocatalytic oxidation of NO (Reproduced with permission from Ref. [88]. Copyright 2020 Elsevier)

CO_2 reduction [95, 96], and hydrogen or H_2O_2 production [97, 98]. The introduction of bias voltage into the working system can further improve the performance of the photocatalytic reaction because of the efficient transfer of photogenerated carriers. However, the photocatalyst in powder form cannot be easily recovered and is easy to scatter and be inhaled by the human body, among other shortcomings. Coating photocatalysts onto the electrodes can overcome such shortcomings of powder catalysts [99]. Presently, most photoelectrocatalytic reactions have been conducted in the liquid phase; thus, introducing an appropriate conductive medium restricts its application to gas phase reaction. Zhang et al. [92, 100] established a reasonable photoelectrocatalytic system to serve as the gas–solid phase reactor for removing NO indoor gas. In 2019, Zhang et al. [92] reported an efficient PEC system for the treatment of NO_x through coating TiO_2-nanoribbon/carbon-nanotube composites onto a stainless-steel mesh as the photoelectrode. In this system, carbon nanotubes enhanced the interaction between TiO_2 and the stainless-steel skeleton, and thus, accelerated the transfer of photoelectrons to the auxiliary electrolytic cell for reduction reaction. Therefore, under ultraviolet irradiation, this PEC system can remove indoor NO gas (550 ppb) at a rate of more than 60%, with a high selectivity to nitrate. As shown in Fig. 11a, the photogenerated electrons quickly separated from the holes and transferred to the counter electrode (Pt), thereby allowing the photogenerated holes to oxidize NO molecules on the stainless-steel electrode under light irradiation at a small bias voltage. Such a PEC reactor was approved for use to effectively remove dry or wet NO; a trace amount of water can increase its efficiency [92]. However, the resistance at the interfaces between the catalysts and the substrate also affected the NO_x removal efficiency because the high resistance often required a large bias voltage to

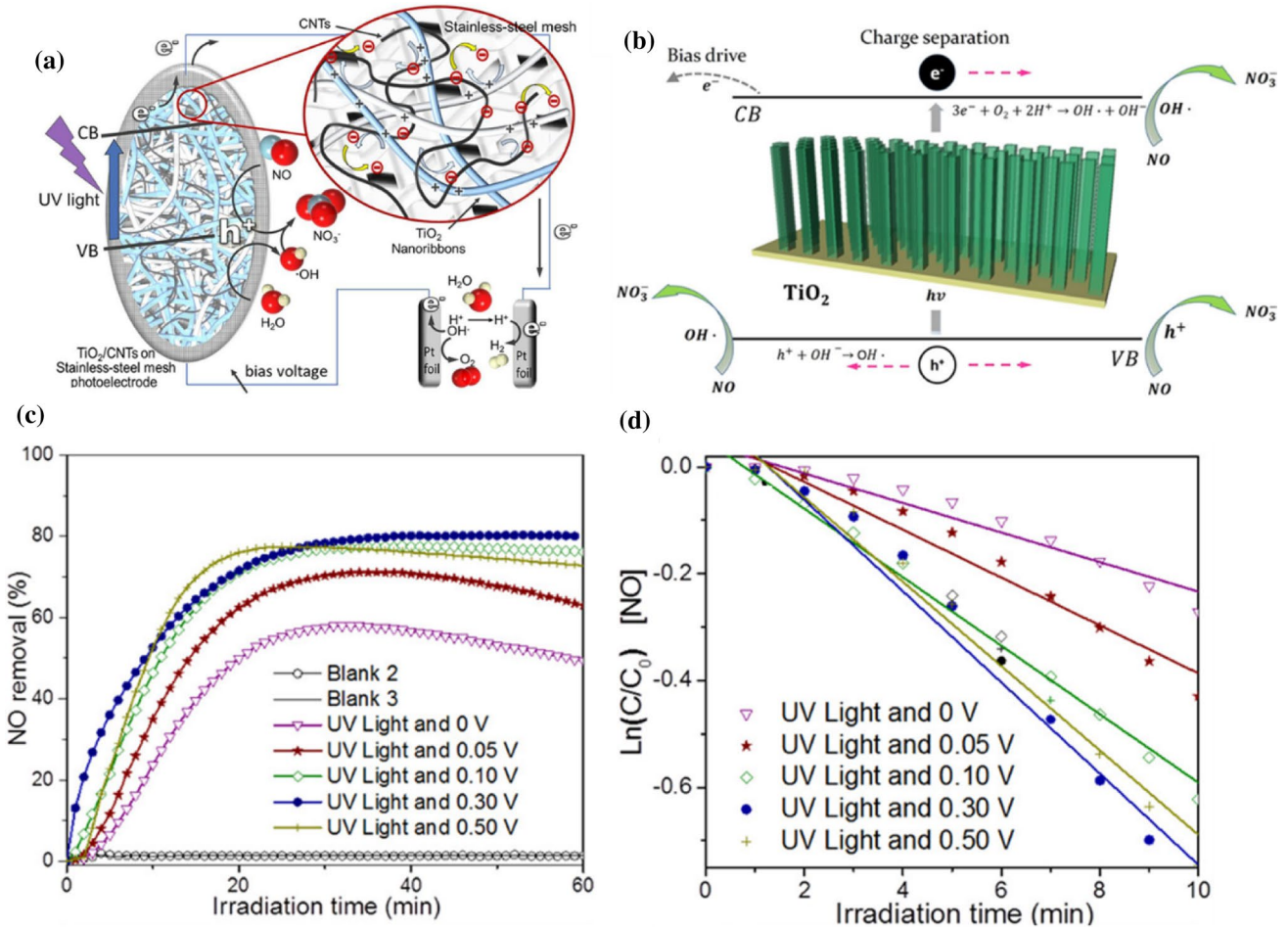

Fig. 11 Schematic illustration of the possible PEC mechanism of CT-25 for the oxidation of NO **a** (Reproduced with permission from Ref. [92]. Copyright 2019 American Chemical Society); and the PC principle of TiO_2 nano-arrays **b**; **c** reaction profiles of the PEC NO oxidation on TF190 (TiO_2 is synthesized at 190 °C) with different bias voltages under UV light (8×4 W LED, 365 nm) irradiation; **d** dependence of ln (C/C_0) on irradiation time (Reproduced with permission from Ref. [100]. Copyright 2020 American Chemical Society)

overcome [101]. To solve the resistance problems, Zhang et al. [100] used FTO glass to act as microwave antennae and generated local superhot spots under microwave conditions (Fig. 11b). In that case, the titanium oxide nanoarray was grown in situ onto FTO glass, thus, solving the problem of insufficient interface contact and large resistance. At low bias voltage (0.3 V), the prepared photoanode had the optimal kinetic constants and the oxidation removal rate of 80% for NO (550 ppb) under illumination (Fig. 11c, d); this rate is much higher than that of the traditional PC process. Considering the symbiosis between photogenerated electrons and holes, the decoupling mechanism of the photogenerated carrier effect should be studied to solve the above key scientific problems. Therefore, our decoupling strategy is to introduce an external electric field to quickly transfer the photogenerated electrons to the counter electrode; this is the basis for the design of the gas-phase photoelectrocatalytic oxidation of NO. We found that the photoelectron transferability can be effectively regulated by adjusting the voltage of the external electric field. When the voltage was increased from 0 to 0.3 V, the nitric oxide removal efficiency significantly increased from 58% to 83% (Fig. 11c). To identify the above promotion mechanism, our strategy was to eliminate the effect of OH by introducing a dry gas into the reaction chamber. Hydrogen peroxide was added to the electrolyte as an electron sacrifice agent to annihilate the electrons so that the photogenerated electrons can be transferred to the external circuit faster to increase the concentration of holes.

Higher hole concentration in the gas-phase photoelectric process is beneficial to the formation of NO_3^- (Fig. 12a), indicating that the hole concentration is crucial for the removal of nitric oxide because, with the increase in hole concentration, the rate constant of nitric oxide removal significantly increases (Fig. 12b). However, with the prolongation of reaction time, the production rate of NO_2 gradually increased (Fig. 12c). To address this challenge, H_2O was introduced into the gas–solid phase photoelectric NO oxidation process to demonstrate the catalytic effect of H_2O. The NO_2 production rate was significantly reduced in H_2O (Fig. 12c). This reduction occurred because the existence of H_2O is conducive to the generation of OH so that the generation of O^{2-} is inhibited, thereby promoting the main NO_3^- reaction [77, 102]. Furthermore, the removal efficiency of NO significantly improved in H_2O compared with that in the absence of H_2O, indicating that there is a significant synergistic effect between the hydroxyl radical and hole concentration for inhibiting the generation of NO_2 in the gas–solid phase photoelectric NO oxidation.

Conclusion and Future Outlook

With the continuous NO_x emissions from the activities of human beings, the development of methods to efficiently eliminate low-concentration NO_x is of growing importance. The photocatalytic oxidation of NO_x has been proved to be an effective method in recent years, and extensive efforts have been devoted to developing highly efficient photocatalysts. In this review, we described the mechanism of photocatalytic oxidation of NO_x and analyzed the key factors for developing highly active photocatalysts. The recent progress on the development of photocatalysts was summarized based

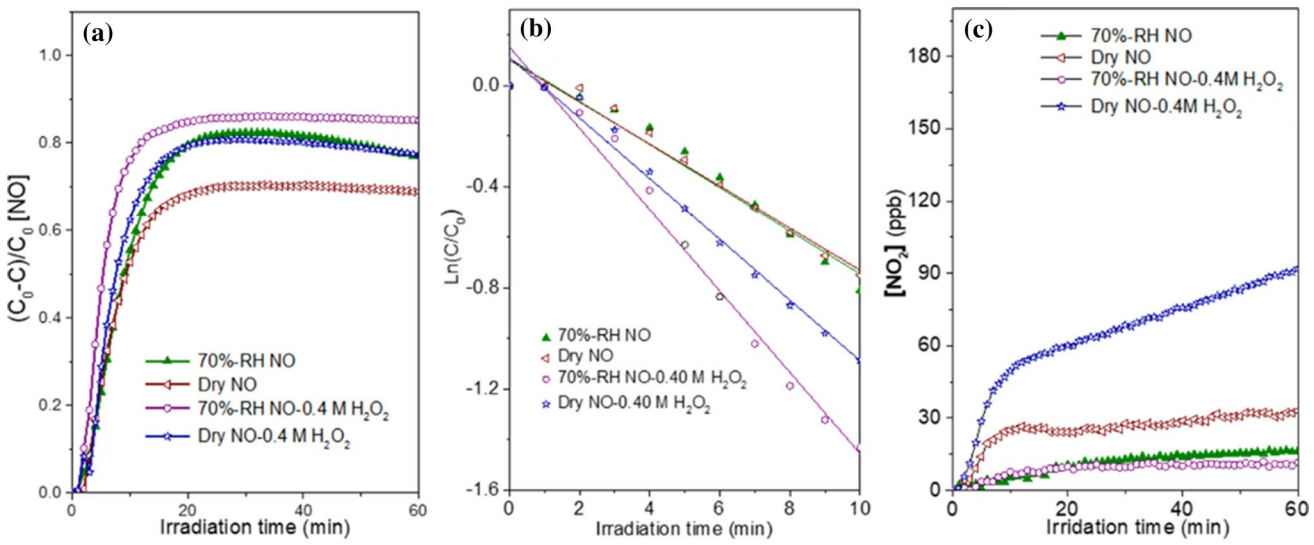

Fig. 12 **a** PEC oxidation of NO for TF190 under UV light irradiation with a 0.3 V bias voltage (70% RH NO, dry NO, 70% RH NO-0.40 M H_2O_2, dry NO-0.40 M H_2O_2), **b** dependence of $\ln(C/C_0)$ on irradiation time, and **c** dependence of NO_2 formation on irradiation time (R eproduced with permission from Ref. [100]. Copyright 2020 American Chemical Society)

on the categories of oxide inorganic semiconductors, Bi-based inorganic semiconductors, the g-C_3N_4 system, and MOFs. With the application of external voltage, the photoelectrocatalytic oxidation of NO_x, in general, possesses higher NO_x removal efficiency than PC alone; recent progress in its development was also reviewed. The research progress of both photocatalytic and photoelectrocatalytic technology was reviewed, and the photocatalytic oxidation and photoelectrocatalytic oxidation mechanisms of NO_x were elucidated in detail. The modification and processing of inorganic photocatalysts, the design of new MOF photocatalysts, and the development of photoanode materials and photoelectrocatalytic reaction devices will become important research subjects in the future.

Currently, the photocatalytic oxidation of NO_x can only be driven by UV or visible light; longer wavelength light (infrared light or far-infrared light) cannot be used for driving the NO oxidation process. In the future, designing highly active longer-wavelength light-driving photocatalysts or active layers of photoanodes for oxidizing NO_x will be of great significance. In addition, achieving the synergistic degradation of NO_x, O_3, and VOCs in the case of complex atmospheric conditions is vital. This synergy will also play an important role in promoting the large-scale environmental application of indoor air pollution control and air purification filters in the future.

Acknowledgements This work was supported by the National Key Research and Development Program of China (No. 2020YFA0211004), and National Natural Science Foundation of China (Nos. 21876112, 21876113, 22022608), Shanghai Engineering Research Center of Green Energy Chemical Engineering and Shanghai Government (No. 18SG41), "111" Innovation and Talent Recruitment Base on Photochemical and Energy Materials (No. D18020).

References

1. Lewis A, Edwards P (2016) Validate personal air-pollution sensors. Nature 535(7610):29–31
2. Ruiz-López MF, Martins-Costa MTC, Anglada JM et al (2019) A new mechanism of acid rain generation from HOSO at the air-water interface. J Am Chem Soc 141(42):16564–16568
3. Krajick K (2001) Acid rain: long-term data show lingering effects from acid rain. Science 292(5515):195–196
4. Glasson WA (1983) Reply to comment on "Effect of hydrocarbon and nitrogen oxide (NO_x) on photochemical smog formation under simulated transport conditions". Environ Sci Technol 17(1):62–63
5. Huebert BJ (1974) Computer modeling of photochemical smog formation. J Chem Educ 51(10):644
6. Ye X, Ma SG, Jiang X et al (2019) The adsorption of acidic gaseous pollutants on metal and nonmetallic surface studied by first-principles calculation: a review. Chin Chem Lett 30(12):2123–2131
7. Buysse CE, Kaulfus A, Nair U et al (2019) Relationships between particulate matter, ozone, and nitrogen oxides during urban smoke events in the western US. Environ Sci Technol 53(21):12519–12528
8. Gao HO, Niemeier DA (2008) Using functional data analysis of diurnal ozone and NO_x cycles to inform transportation emissions control. Transp Res Part D Transp Environ 13(4):221–238
9. Lelieveld J, Evans JS, Fnais M et al (2015) The contribution of outdoor air pollution sources to premature mortality on a global scale. Nature 525(7569):367–371
10. Zhao CN, Xu Z, Wu GC et al (2019) Emerging role of air pollution in autoimmune diseases. Autoimmun Rev 18(6):607–614
11. Schraufnagel DE, Balmes JR, Cowl CT et al (2019) Air pollution and noncommunicable diseases: a review by the forum of international respiratory societies' environmental committee, part 2: air pollution and organ systems. Chest 155(2):417–426
12. Rezaei F, Rownaghi AA, Monjezi S et al (2015) SO_x/NO_x removal from flue gas streams by solid adsorbents: a review of current challenges and future directions. Energy Fuels 29(9):5467–5486
13. Blejchař T, Konvička J, von der Heide B et al (2018) High temperature modification of SNCR technology and its impact on NO_x removal process. EPJ Web Conf 180:02009
14. Damma D, Ettireddy P, Reddy B et al (2019) A review of low temperature NH_3-SCR for removal of NO_x. Catalysts 9(4):349
15. Schill L, Fehrmann R (2018) Strategies of coping with deactivation of NH_3-SCR catalysts due to biomass firing. Catalysts 8(4):135
16. Chen CM, Cao Y, Liu ST et al (2018) Review on the latest developments in modified vanadium-titanium-based SCR catalysts. Chin J Catal 39(8):1347–1365
17. Pu YJ, Xie XY, Jiang WJ et al (2020) Low-temperature selective catalytic reduction of NO_x with NH_3 over zeolite catalysts: a review. Chin Chem Lett 31(10):2549–2555
18. Park JH, Ahn JW, Kim KH et al (2019) Historic and futuristic review of electron beam technology for the treatment of SO_2 and NO_x in flue gas. Chem Eng J 355:351–366
19. Gholami F, Tomas M, Gholami Z et al (2020) Technologies for the nitrogen oxides reduction from flue gas: a review. Sci Total Environ 714:136712
20. Dong F, Zhao Z, Sun Y et al (2015) An advanced semimetal–organic Bi spheres–*g*-C_3N_4 nanohybrid with SPR-enhanced visible-light photocatalytic performance for NO purification. Environ Sci Technol 49(20):12432–12440
21. Wang H, Sun YJ, Jiang GM et al (2018) Unraveling the mechanisms of visible light photocatalytic NO purification on earth-abundant insulator-based core-shell heterojunctions. Environ Sci Technol 52(3):1479–1487
22. Ni ZL, Sun YJ, Zhang YX et al (2016) Fabrication, modification and application of $(BiO)_2CO_3$-based photocatalysts: a review. Appl Surf Sci 365:314–335
23. Ibusuki T, Takeuchi K (1994) Removal of low concentration nitrogen oxides through photoassisted heterogeneous catalysis. J Mol Catal 88(1):93–102

24. Wang KH, Tsai HH, Hsieh YH (1998) A study of photocatalytic degradation of trichloroethylene in vapor phase on TiO_2 photocatalyst. Chemosphere 36(13):2763–2773
25. Yang JS, Liao WP, Wu JJ (2013) Morphology and interfacial energetics controls for hierarchical anatase/rutile TiO_2 nanostructured array for efficient photoelectrochemical water splitting. ACS Appl Mater Interfaces 5(15):7425–7431
26. Huy TH, Bui DP, Kang F et al (2019) SnO_2/TiO_2 nanotube heterojunction: the first investigation of NO degradation by visible light-driven photocatalysis. Chemosphere 215:323–332
27. Sun ML, Li JY, Dong F (2020) Structure control methods of Bi based photocatalytic materials and research progress on their application in environmental energy field. J Huazhong Agri Uni 39(5):17–25 (**(in Chinese)**)
28. Zhu S, Lu L, Zhao Z et al (2017) Mesoporous Ni-doped δ-Bi_2O_3 microspheres for enhanced solar-driven photocatalysis: a combined experimental and theoretical investigation. J Phys Chem C 121(17):9394–9401
29. Wang X, Maeda K, Thomas A et al (2009) A metal-free polymeric photocatalyst for hydrogen production from water under visible light. Nat Mater 8(1):76–80
30. Zhu W, Liu PJ, Xiao SN et al (2015) Microwave-assisted synthesis of Ag-doped MOFs-like organotitanium polymer with high activity in visible-light driven photocatalytic NO oxidization. Appl Catal B Environ 172–173:46–51
31. Gong XQ, Selloni A (2005) Reactivity of anatase TiO_2 nanoparticles: the role of the minority (001) surface. J Phys Chem B 109(42):19560–19562
32. Selloni A (2008) Crystal growth-anatase shows its reactive side. Nat Mater 7(8):613–615
33. Wu BH, Guo CY, Zheng NF et al (2008) Nonaqueous production of nanostructured anatase with high-energy facets. J Am Chem Soc 130(51):17563–17567
34. Yang HG, Liu G, Qiao SZ et al (2009) Solvothermal synthesis and photoreactivity of anatase TiO2 nanosheets with dominant 001 facets. J Am Chem Soc 131(11):4078–4083
35. Li GX, Fang K, Ou Y et al (2021) Surface study of the reconstructed anatase TiO_2 (001) surface. Prog Nat Sci Mater Int 31(1):1–13
36. Yang HG, Sun CH, Qiao SZ et al (2008) Anatase TiO_2 single crystals with a large percentage of reactive facets. Nature 453(7195):638–641
37. Han X, Kuang Q, Jin M et al (2009) Synthesis of titania nanosheets with a high percentage of exposed (001) facets and related photocatalytic properties. J Am Chem Soc 131(9):3152–3153
38. Chen L, Yang SD, Zhang Q et al (2021) Rational design of {0 0 1}-faceted TiO_2 nanosheet arrays/graphene foam with superior charge transfer interfaces for efficient photocatalytic degradation of toxic pollutants. Sep Purif Technol 265:118444
39. Duan YY, Luo JM, Zhou SC et al (2018) TiO_2-supported Ag nanoclusters with enhanced visible light activity for the photocatalytic removal of NO. Appl Catal B Environ 234:206–212
40. Martinez-Oviedo A, Ray SK, Joshi B et al (2020) Enhancement of NO_x photo-oxidation by Fe- and Cu-doped blue TiO_2. Environ Sci Pollut Res 27(21):26702–26713
41. Xiao SN, Zhang DQ, Pan DL et al (2019) A chloroplast structured photocatalyst enabled by microwave synthesis. Nat Commun 10:1570
42. He Y, Li JY, Li KL et al (2020) Bi quantum dots implanted 2D C-doped BiOCl nanosheets: enhanced visible light photocatalysis efficiency and reaction pathway. Chin J Catal 41(9):1430–1438
43. Lei B, Cui W, Sheng JP et al (2020) Synergistic effects of crystal structure and oxygen vacancy on Bi_2O_3 polymorphs: intermediates activation, photocatalytic reaction efficiency, and conversion pathway. Sci Bull 65(6):467–476
44. Dong F, Wang Z, Li Y et al (2014) Immobilization of polymeric g-C_3N_4 on structured ceramic foam for efficient visible light photocatalytic air purification with real indoor illumination. Environ Sci Technol 48(17):10345–10353
45. He WJ, Sun YJ, Jiang GM et al (2018) Activation of amorphous Bi_2WO_6 with synchronous Bi metal and Bi_2O_3 coupling: photocatalysis mechanism and reaction pathway. Appl Catal B: Environ 232:340–347
46. Hu J, Chen D, Mo Z et al (2019) Z-scheme 2D/2D heterojunction of black phosphorus/monolayer Bi_2WO_6 nanosheets with enhanced photocatalytic activities. Angew Chem Int Ed Engl 58(7):2073–2077
47. Cheng HF, Huang BB, Dai Y (2014) Engineering BiOX (X = Cl, Br, I) nanostructures for highly efficient photocatalytic applications. Nanoscale 6(4):2009–2026
48. Li J, Yu Y, Zhang LZ (2014) Bismuth oxyhalide nanomaterials: layered structures meet photocatalysis. Nanoscale 6(15):8473–8488
49. Ye LQ, Su YR, Jin XL et al (2014) Recent advances in BiOX (X = Cl, Br and I) photocatalysts: synthesis, modification, facet effects and mechanisms. Environ Sci: Nano 1(2):90–112
50. Zhang HJ, Liu L, Zhou Z (2012) Towards better photocatalysts: first-principles studies of the alloying effects on the photocatalytic activities of bismuth oxyhalides under visible light. Phys Chem Chem Phys 14(3):1286–1292
51. Zhang HJ, Liu L, Zhou Z (2012) First-principles studies on facet-dependent photocatalytic properties of bismuth oxyhalides (BiOXs). RSC Adv 2(24):9224–9229
52. Wang L, Lv D, Dong F et al (2019) Boosting visible-light-driven photo-oxidation of BiOCl by promoted charge separation via vacancy engineering. ACS Sustain Chem Eng 7(3):3010–3017
53. Lv Y, Zhu YY, Zhu YF (2013) Enhanced photocatalytic performance for the $BiPO_{4-x}$ nanorod induced by surface oxygen vacancy. J Phys Chem C 117(36):18520–18528
54. Liu YF, Lv Y, Zhu YY et al (2014) Fluorine mediated photocatalytic activity of $BiPO_4$. Appl Catal B: Environ 147:851–857
55. Li JY, Dong XA, Sun YJ et al (2018) Facet-dependent interfacial charge separation and transfer in plasmonic photocatalysts. Appl Catal B Environ 226:269–277
56. Wang H, Yuan XZ, Wu Y et al (2017) Plasmonic Bi nanoparticles and BiOCl sheets as cocatalyst deposited on perovskite-type $ZnSn(OH)_6$ microparticle with facet-oriented polyhedron for improved visible-light-driven photocatalysis. Appl Catal B: Environ 209:543–553
57. Fang WJ, Jiang Z, Yu L et al (2017) Novel dodecahedron $BiVO_4$: YVO_4 solid solution with enhanced charge separation on adjacent exposed facets for highly efficient overall water splitting. J Catal 352:155–159
58. Jiang GM, Li XW, Lan MN et al (2017) Monodisperse bismuth nanoparticles decorated graphitic carbon nitride: enhanced visible-light-response photocatalytic NO removal and reaction pathway. Appl Catal B Environ 205:532–540
59. Li JR, Zhang WD, Ran MX et al (2019) Synergistic integration of Bi metal and phosphate defects on hexagonal and monoclinic $BiPO_4$: enhanced photocatalysis and reaction mechanism. Appl Catal B Environ 243:313–321
60. Greaves C, Blower SK (1988) Structural relationships between $Bi_2O_2CO_3$ and β-Bi_2O_3. Mater Res Bull 23(7):1001–1008
61. Lu YF, Huang Y, Zhang YF et al (2019) Effects of H_2O_2 generation over visible light-responsive $Bi/Bi_2O_{2-x}CO_3$ nanosheets on their photocatalytic NO_x removal performance. Chem Eng J 363:374–382

62. Xiong T, Cen WL, Zhang YX et al (2016) Bridging the g-C_3N_4 interlayers for enhanced photocatalysis. ACS Catal 6(4):2462–2472
63. Wang D, Saleh NB, Sun W et al (2019) Next-generation multifunctional carbon-metal nanohybrids for energy and environmental applications. Environ Sci Technol 53(13):7265–7287
64. Li K, He Y, Chen P et al (2020) Theoretical design and experimental investigation on highly selective Pd particles decorated C_3N_4 for safe photocatalytic NO purification. J Hazard Mater 392:122357
65. Chen ZF, Lu SC, Wu QL et al (2018) Salt-assisted synthesis of 3D open porous g-C_3N_4 decorated with cyano groups for photocatalytic hydrogen evolution. Nanoscale 10(6):3008–3013
66. He F, Chen G, Zhou Y et al (2015) The facile synthesis of mesoporous g-C_3N_4 with highly enhanced photocatalytic H_2 evolution performance. Chem Commun (Camb) 51(90):16244–16246
67. Raziq F, Qu Y, Humayun M et al (2017) Synthesis of SnO_2/B-P codoped g-C_3N_4 nanocomposites as efficient cocatalyst-free visible-light photocatalysts for CO_2 conversion and pollutant degradation. Appl Catal B Environ 201:486–494
68. Fu YS, Huang T, Jia BQ et al (2017) Reduction of nitrophenols to aminophenols under concerted catalysis by Au/g-C_3N_4 contact system. Appl Catal B Environ 202:430–437
69. Zhou M, Dong GH, Yu FK et al (2019) The deep oxidation of NO was realized by Sr multi-site doped g-C_3N_4 via photocatalytic method. Appl Catal B Environ 256:117825
70. Zhang ZZ, Xu MK, Ho W et al (2016) Simultaneous excitation of $PdCl_2$ hybrid mesoporous g-C_3N_4 molecular/solid-state photocatalysts for enhancing the visible-light-induced oxidative removal of nitrogen oxides. Appl Catal B Environ 184:174–181
71. Yang Y, Zhang Q, Zhang R et al (2018) Compressible and recyclable monolithic g-C_3N_4/melamine sponge: a facile ultrasonic-coating approach and enhanced visible-light photocatalytic activity. Front Chem 6:156
72. Liu YW, Xiao C, Li Z et al (2016) Vacancy engineering for tuning electron and phonon structures of two-dimensional materials. Adv Energy Mater 6(23):1600436
73. Wang Z, Huang Y, Chen M et al (2019) Roles of N-vacancies over porous g-C_3N_4 microtubes during photocatalytic NO_x removal. ACS Appl Mater Interfaces 11(11):10651–10662
74. Liao JZ, Cui W, Li JY et al (2020) Nitrogen defect structure and NO+ intermediate promoted photocatalytic NO removal on H_2 treated g-C_3N_4. Chem Eng J 379:122282
75. Ma JZ, Wang CX, He H (2016) Enhanced photocatalytic oxidation of NO over g-C_3N_4-TiO_2 under UV and visible light. Appl Catal B Environ 184:28–34
76. Tian N, Zhang YH, Liu CY et al (2016) G-C_3N_4/$Bi_4O_5I_2$ 2D–2D heterojunctional nanosheets with enhanced visible-light photocatalytic activity. RSC Adv 6(13):10895–10903
77. Shang H, Li M, Li H et al (2019) Oxygen vacancies promoted the selective photocatalytic removal of NO with blue TiO_2 via simultaneous molecular oxygen activation and photogenerated hole annihilation. Environ Sci Technol 53(11):6444–6453
78. Dong F, Li QY, Sun YJ et al (2014) Noble metal-like behavior of plasmonic Bi particles as a cocatalyst deposited on $(BiO)_2CO_3$ microspheres for efficient visible light photocatalysis. ACS Catal 4(12):4341–4350
79. Hu JD, Chen DY, Li NJ et al (2018) 3D aerogel of graphitic carbon nitride modified with perylene imide and graphene oxide for highly efficient nitric oxide removal under visible light. Small 14(19):1800416
80. Han X, Godfrey HGW, Briggs L et al (2018) Reversible adsorption of nitrogen dioxide within a robust porous metal–organic framework. Nat Mater 17(8):691–696
81. Li J, Han X, Zhang X et al (2019) Capture of nitrogen dioxide and conversion to nitric acid in a porous metal-organic framework. Nat Chem 11(12):1085–1090
82. Zeng L, Guo XY, He C et al (2016) Metal-organic frameworks: versatile materials for heterogeneous photocatalysis. ACS Catal 6(11):7935–7947
83. Zhang T, Lin W (2014) Metal-organic frameworks for artificial photosynthesis and photocatalysis. Chem Soc Rev 43(16):5982–5993
84. Li SL, Xu Q (2013) Metal-organic frameworks as platforms for clean energy. Energy Environ Sci 6(6):1656–1683
85. Stock N, Biswas S (2012) Synthesis of metal-organic frameworks (MOFs): routes to various MOF topologies, morphologies, and composites. Chem Rev 112(2):933–969
86. Zhou HCJ, Kitagawa S (2014) Metal-organic frameworks (MOFs). Chem Soc Rev 43(16):5415–5418
87. Li XR, Le ZY, Chen XL et al (2018) Graphene oxide enhanced amine-functionalized titanium metal organic framework for visible-light-driven photocatalytic oxidation of gaseous pollutants. Appl Catal B Environ 236:501–508
88. Chen XL, Cai Y, Liang R et al (2020) NH_2-UiO-66(Zr) with fast electron transfer routes for breaking down nitric oxide via photocatalysis. Appl Catal B: Environ 267:118687
89. Li GS, Zhang DQ, Yu JC (2008) Ordered mesoporous $BiVO_4$ through nanocasting: a superior visible light-driven photocatalyst. Chem Mater 20(12):3983–3992
90. Huang Y, Ho W, Lee S et al (2008) Effect of carbon doping on the mesoporous structure of nanocrystalline titanium dioxide and its solar-light-driven photocatalytic degradation of NO_x. Langmuir 24(7):3510–3516
91. Cui W, Li J, Dong F et al (2017) Highly efficient performance and conversion pathway of photocatalytic NO oxidation on SrO-Clusters@Amorphous carbon nitride. Environ Sci Technol 51(18):10682–10690
92. Xiao SN, Wan Z, Zhou JC et al (2019) Gas-phase photoelectrocatalysis for breaking down nitric oxide. Environ Sci Technol 53(12):7145–7154
93. Fujishima A, Honda K (1972) Electrochemical photolysis of water at a semiconductor electrode. Nature 238(5358):37–38
94. Ma TY, Dai S, Jaroniec M et al (2014) Metal-organic framework derived hybrid Co_3O_4-carbon porous nanowire arrays as reversible oxygen evolution electrodes. J Am Chem Soc 136(39):13925–13931
95. Sun JY, Guo YP, Wang Y et al (2018) H_2O_2 assisted photoelectrocatalytic degradation of diclofenac sodium at g-C_3N_4/$BiVO_4$ photoanode under visible light irradiation. Chem Eng J 332:312–320
96. Qi Y, Xu Q, Wang Y et al (2016) CO_2-induced phase engineering: protocol for enhanced photoelectrocatalytic performance of 2D MoS_2 nanosheets. ACS Nano 10(2):2903–2909
97. Xie S, Zhang Q, Liu G et al (2016) Photocatalytic and photoelectrocatalytic reduction of CO_2 using heterogeneous catalysts with controlled nanostructures. Chem Commun (Camb) 52(1):35–59
98. Daghrir R, Drogui P, El Khakani MA (2013) Photoelectrocatalytic oxidation of chlortetracycline using Ti/TiO_2 photo-anode with simultaneous H_2O_2 production. Electrochim Acta 87:18–31
99. Leng WH, Zhu WC, Ni J et al (2006) Photoelectrocatalytic destruction of organics using TiO_2 as photoanode with simultaneous production of H_2O_2 at the cathode. Appl Catal A Gen 300(1):24–35
100. Dai WR, Tao Y, Zou HJ et al (2020) Gas-phase photoelectrocatalytic oxidation of NO via TiO_2 nanorod array/FTO photoanodes. Environ Sci Technol 54(9):5902–5912
101. Hoet PH, Brüske-Hohlfeld I, Salata OV (2004) Nanoparticles-known and unknown health risks. J Nanobiotechnology 2(1):12
102. Li H, Shang H, Cao X et al (2018) Oxygen vacancies mediated complete visible light NO oxidation via side-on bridging superoxide radicals. Environ Sci Technol 52(15):8659–8665

Dieqing Zhang received her PhD degree in 2010 at the Chinese University of Hong Kong, China. Now she is a professor and Master Tutor of Shanghai Normal University and International Joint Laboratory of Resource Chemistry. Her actual interests is air pollution control. She has won the first prize of Shanghai Natural Science Award (5/5) and has been selected to support talent programs such as Shanghai Top Young Talents Program, Shuguang Scholar, Young Science and Technology Starlight, and Pujiang Scholar. She presided over the National Science Foundation for Excellent Young People in 2020.